Research Article Vol. 62, No. 11 / 10 April 2023 / Applied Optics 2815

applied optics

Pinholes in Al/MgF_2

Xiaodong Wang,* Peng Zhou, Shuai Ren, Haifeng Wang, Xinkai Li, and Bo Chen

Changchun Institute of Optics, Fine Mechanics and Physics, Chinese Academy of Sciences, Changchun 130033, China
**wangxiaodong@ciomp.ac.cn*

Received 26 January 2023; revised 10 March 2023; accepted 16 March 2023; posted 20 March 2023; published 3 April 2023

Pinholes in Al/MgF_2 were first inferred by the transmittance enhancement in Larruquert group's research. However, no direct proof was reported to verify the existence of the pinholes in Al/MgF_2. In the past 80 years, pinholes were first observed by dark-field microscopy and bright-field microscopy in the transmission mode. They were small and on the order of several hundred nanometers to several micrometers. Essentially, the pinhole was not a real hole, partially because of the lack of the Al element. Increasing the thickness of Al cannot reduce the size of the pinholes. The occurrence of the pinholes was dependent on the deposition rate of the Al film and the substrate heating temperature, and it was independent of the substrate materials. This research eliminates an otherwise easily ignored scattering source, and it will benefit the development of ultra-precise optics, including mirrors for gyro-lasers, the detection of gravitational waves, and coronagraph detection.

https://doi.org/10.1364/AO.486210

1. INTRODUCTION

The absorption edge of aluminum (Al) is around 80 nm, and it shows a broadband high reflectance from far ultraviolet (FUV) to the infrared region [1]. To avoid the oxidation, magnesium fluoride (MgF_2) with an absorption edge of 115 nm was used to overcoat on the Al films [2–4]. Aluminum fluoride (AlF_3) had a shorter cutoff wavelength of 113 nm and less stress, and it was used to replace the MgF_2 as the protective layer of the Al film [5]. Lithium fluoride (LiF) has the shortest cutoff wavelength of 102 nm in nature, and it can extend the reflectance region of Al film to the wavelength of 102 nm. Al/LiF was used in the Far Ultraviolet Spectroscopic Explorer (FUSE). Because LiF was hygroscopic [6–14], the reflectance of Al/LiF mirrors for the FUSE still decreased from 70% to 55% by the launch in the short FUV wavelengths, even though considerable care was taken in humidity control during the test and assembly procedures [13]. Hence, multilayer protective materials were used to protect the Al films. Quijada proposed a novel room-temperature reactive physical vapor deposition (rPVD) process to produce Al/LiF. Al and LiF were immediately exposed to the reactive xenon di-fluoride (XeF_2) gas after they were deposited by conventional PVD. In fact, this coating had a structure of Al/(2.5−3.2 nm)AlF_3/LiF and exhibited an unprecedented reflectance of 92.6% at 121.6 nm. This coating fabricated with the rPVD process demonstrated more durable and less hygroscopic than those coated by the standard PVD process [12]. Marcos deposited Al/LiF by thermal evaporation at room temperature and post-annealed at elevated temperatures (265–285°C), then coated MgF_2 by atomic layer deposition (ALD). Mirrors with a reflectance of 70% at 103 nm were achieved [11]. The ALD method was used to deposit metal fluoride materials of MgF_2, AlF_3, and LiF to protect the Al film [14–16]. Ultrathin protective material meant less absorption loss and allowed the mirrors to approach the ideal Al intrinsic reflectivity of 90–115 nm [15,16]. Their calculations suggested that significant performance advantages in the region of 90 to 105 nm may be possible with these ultrathin layers [15]. A Ti seed layer was deposited before Al/MgF_2 deposition, this layer had a positive influence on the wetting behavior, and surface roughness of the Al films was significantly reduced to be 0.34 nm. A reflectance enhancement at 120–200 nm was achieved and, particularly, the reflectance dip centered at around 160 nm was almost completely removed because a Ti seed film as thin as 1 nm provided the largest surface plasmon absorption reduction [17,18].

Al/MgF_2 was widely used in many optical payloads, such as a wide-field auroral imager on board the Fengyun satellite [19], an ultraviolet imager on board the Polar satellite [20], Lyman-alpha Solar Telescope [21], and Hubble Space Telescope [22]. If Al was deposited on a "hot" substrate, surface roughness was high, and the reflectance was low. Hence, Al must be deposited on a "cold" substrate. At the beginning, Al and MgF_2 were deposited at room temperature [23,24], and this coating process was called cold deposition or a two-step method. For samples deposited by this process, MgF_2 has a high absorption, and a low pack density. Some of the water or air was prone to penetrate the MgF_2 film, and this led to the degradation in the reflectance of Al/MgF_2. To enhance its spectral stability, the fabrication method was modified from a two-step to be a three-step method proposed by Quijada [8]. Al was deposited at room temperature; immediately, an MgF_2 layer around 4.5 nm was coated to protect Al from oxidation; then substrate heating temperature increased to an optimal value; finally, remanent MgF_2 was

deposited [25,26]. An optimal substrate heating temperature was discussed, and pinhole defects were first mentioned in Ref. [16]. The existence of pinholes was inferred by the transmittance enhancement. However, they did not observe pinholes by bright-field optical microscopy [25,26]. The existence of pinholes means that the transmittance is high at some spot, and this will lead to a light leak in a reflective mirror. The pinhole is also a defect like a particle or crater, and it is a light-scattering source [27,28]. The pinhole is prone to absorb water or air, and it will alter the refractive of thin films. Here pinholes were first observed by dark-field optical microscopy and bright-field optical microscopy in the transmission mode, and the structure of the pinholes was analyzed.

2. DEPOSITION AND CHARACTERIZATION

Al/MgF_2 was designed by Optilayer software (version 10.48 h). The purity of Al and MgF_2 was 99.999% and 99.99%, respectively. Before the coating, the substrate was carefully cleaned by an ultrasonic bath, and the ultrasonic frequency was 40 KHz. Then the substrate was dried by the spinning. The cleaning process ensured that less than five particles (larger than 200 nm) per area with a diameter of 1.2 mm on the substrate. The particles on the substrate were counted by dark-field microscopy. Al and MgF_2 were deposited by the thermal evaporation method. Al was deposited by tungsten a, and MgF_2 were fabricated by molybdenum boat with a rate of 0.2 nm/s. The base pressure of the chamber was pumped by a molecular pump to be 3.0×10^{-4} Pa. Al/MgF_2 was produced by the three-step method: Al was deposited at room temperature; immediately, a layer of MgF_2 film with a thickness of 11.0 nm was deposited on the Al film to avoid the oxidation. Then the substrate temperature was heated to be an optimal value. Finally, remanent MgF_2 was deposited. The thickness was controlled by the quartz crystal. Particle contamination was strictly controlled in the substrate cleaning, deposition, and handling to avoid confusing with pinholes.

The reflectance in the FUV region was measured by our own developed reflectometer with a deuterium lamp, and the details about this system can be found in Ref. [29]. The pinholes in Al/MgF_2 were observed by dark-field microscopy (Sunny, RX50M) and bright-field optical microscopy (Mitutoyo, MF-B1010) in the transmission mode; the magnification was 200 and 100, respectively. The pinhole density and size in the pictures were quantitatively determined by ImageJ software. The pinholes were analyzed by the scanning electron microscope (SEM) [ZEISS, Sigma 300].

3. DISCUSSION

Table 1 gives the deposition parameters, density, and size of the pinholes for the samples. As we all know, the high reflectance and good spectral stability will be achieved by increasing the deposition rate of Al and substrate heating temperature when additional MgF_2 is deposited. However, unfortunately, our observation by dark-field microscopy and bright-field microscopy in the transmission mode revealed that these two methods made pinhole phenomena significant.

It was found that no pinholes formed in Al/MgF_2 when Al and MgF_2 were deposited at room temperature. This phenomenon was the as with the viewpoint of Ref. [26]. Figure 1 shows the pinholes in the Al/MgF_2 coating observed by dark-field microscopy (a) and bright-field microscopy in the transmission mode (b). The pinholes, like particles on the coatings, scattered the incoming light, and they were shining like many stars in the sky at night. Figure 1 demonstrated a dependence of the pinhole density and size on deposition rates (c) for samples of D1–D4 and substrate temperature (d) for samples of T1-T2 in Table 1. With the increasing of the deposition rates from 1.1 to 4.2 nm/s and temperature from 220 to 240 deg, the pinhole density decreased, and the pinhole size increased. In other words, with the increasing of the deposition rate of Al and the substrate heating temperature, the pinholes became larger and sparser. Hence, the occurrence of the pinholes was dependence on the deposition rates of Al and the substrate heating temperature.

Figure 2 revealed a dependence of the reflectance (a) and transmittance (b) on the deposition rates for samples of D1–D4 and substrate temperature for Samples of T1-T2 in Table 1, respectively. The wavelength region was from 220 to 760 nm. The reflectance of samples of D1–D4 increased when the deposition rates increased from 1.1 to 3.0 nm/s, and it statured at a deposition rate of 4.2 nm/s. The transmittance of samples decreased when the deposition rates increased from 1.1 to 2.0 nm/s, then increased when the deposition rates increased from 2.0 to 4.2 nm/s. The reflectance of the coatings first increased, then decreased with the increasing of the pinhole

Table 1. Deposition Parameters, and Density and Size of Pinholes of Samples

					Pinholes	
Sample	Al Thickness (nm)	Deposition Rate Al (nm/s)	Temperature (Deg)	Substrate	Density (/mm^2)	Size (nm)
D1	70	1.1	220	Silicon	Yes, 6021	260
D2	70	2.0	220	Silicon	Yes, 5395	269
D3	70	3.0	220	Silicon	Yes, 1027	1000
D4	70	4.2	220	Silicon	Yes, 560	2000
D5	140	1.1	220	Silicon	Yes, 6252	249
T1	70	2.0	220	Silicon	Yes, 5395	269
T2	70	2.0	240	Silicon	Yes, 2241	492
S1	70	2.0	220	Fused Silica	Yes, 5418	258
S2	70	2.0	220	Zerodur	Yes, 5306	276
R1	70	1.0	200	Silicon	No —	—

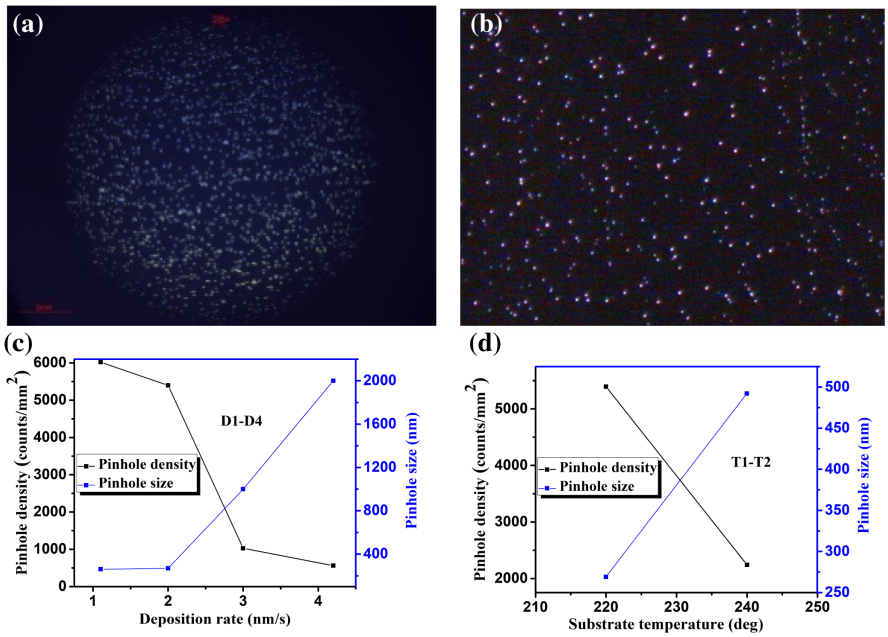

Fig. 1. Pinholes in the Al/MgF_2 coating observed by (a) dark-field microscopy and (b) bright-field microscopy in the transmission mode. (c) Dependence of the pinhole density and size on deposition rates: 1.1, 2.0, 3.0, and 4.2 nm/s. (d) Dependence of the pinhole density and size on the substrate temperature: 220 and 240 deg.

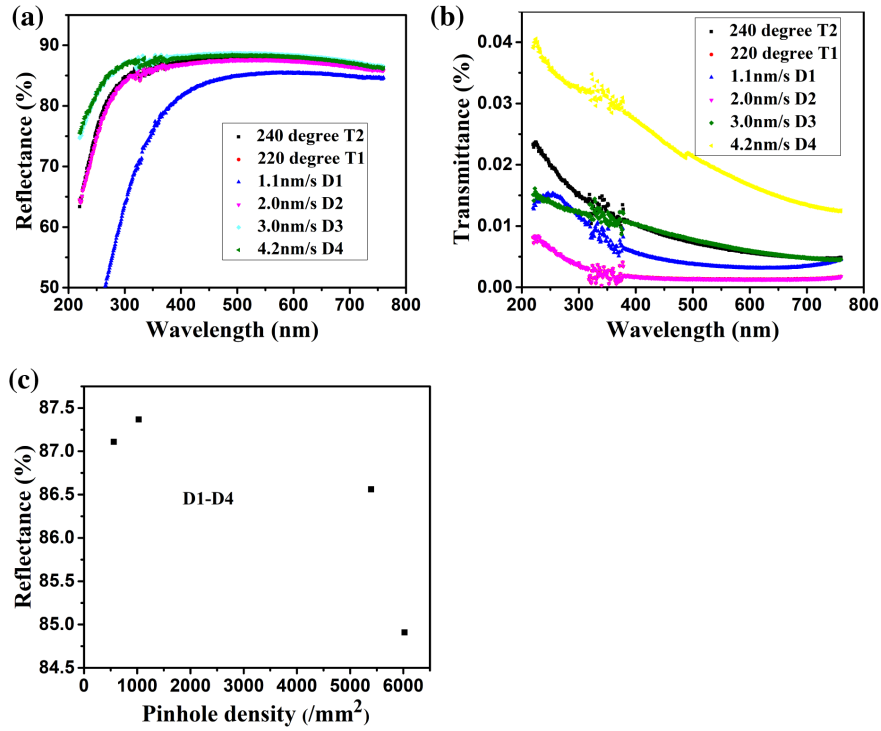

Fig. 2. (a) Reflectance and (b) transmittance curves of samples as function deposition rates of the Al and substrate temperature. (c) Reflectance of samples as a function of the pinhole density.

density [Fig. 2(c)]. The substrate temperature had a negligible influence on the reflectance of the coatings, and the transmittance> increased when the substrate temperature increased from 220 to 240 deg. The existence of the pinholes slowed down the enhancement magnitude of the reflectance, and it led to the transmittance increasing for the coatings. The transmittance measurement indeed was an effectively indirect way to characterize the pinhole [25,26].

We also used three kinds of materials as the substrate for the deposition of Al/MgF_2. As shown in Table 1, samples S1, S2, and D2 used fused silica, Zerodur, silicon as the substrate; the

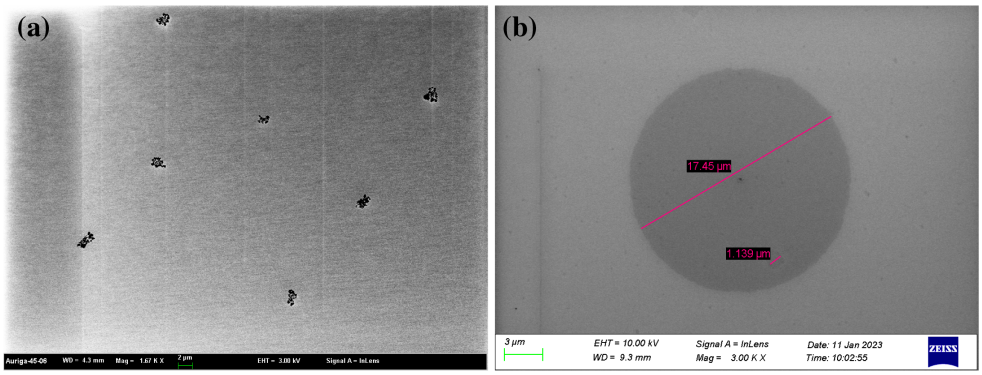

Fig. 3. SEM graph of pinholes in Al/MgF_2.

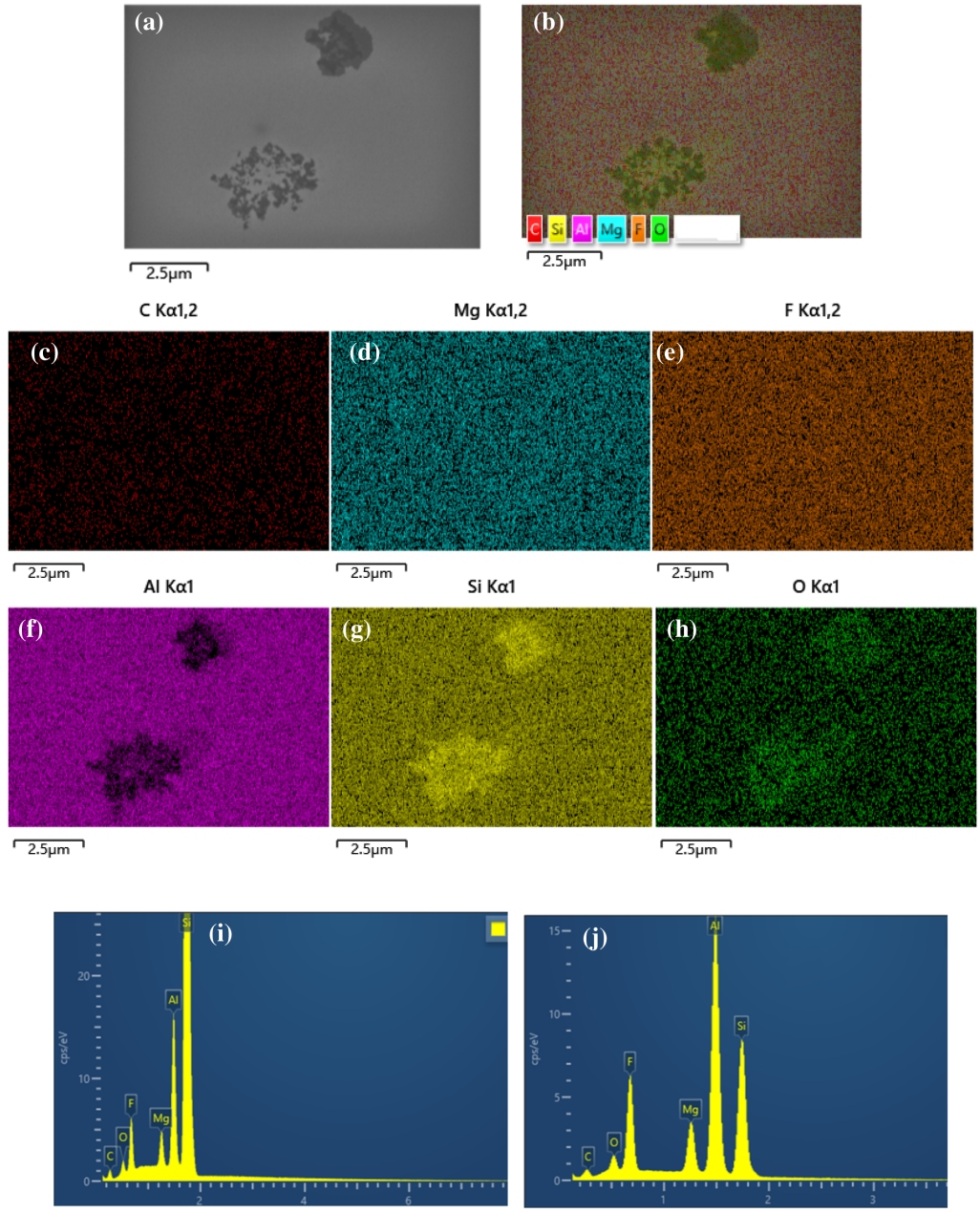

Fig. 4. SEM analysis for the element distribution of the pinhole in the Al/MgF_2 coating: (a) SEM image of the whole, (b) EDS image of the whole, (c) C, (d) Mg, (e) F, (f) Al, (g) Si, and (h) O element distribution maps. EDX plots of the composition (i) inside and (j) outside the pinhole.

deposition rate of Al was 2.0 nm/s, and the substrate temperature was 220 deg. These three samples had pinholes, and the size and density of the pinholes were similar. Hence, the occurrence of the pinholes was independent of the substrate material.

We performed an SEM analysis for the element distribution of the pinhole in the Al/MgF_2 coating. As shown in Fig. 3, the size of the pinholes ranged from several hundred nanometers to several micrometers. Interestingly, most of the pinholes were irregular [Fig. 3(a)], and some pinholes were circular [Fig. 3(b)]. There was a circular shadow area with a diameter of 17.5 μm, a small pinhole with a diameter of 120 nm at its center, and a shallow rectangular pinhole [Fig. 3(b)].

Figures 4(a) and 4(b) indicate the element distribution image and SEM image of the pinhole, respectively, and the other six pictures [Figs. 4(c)–4(h)] show C, Mg, F, Al, Si, and O element distributions, respectively. The C element was the surface contamination. However, there was a hole in the Al element distribution; in other words, there was Al element loss in the pinholes. Mg, F element distributions were uniform. The areas of Si and O elements (the substrate was silicon with a thin oxidation layer) in the pinholes were brighter than other areas. This was because more Si and O can be detected due to Al element loss. Figures 4(i) and 4(j) give the energy dispersive X-ray spectroscopy (EDX) plots of the composition inside and outside the pinhole, respectively. It is obvious that the quantity of the Al element inside the pinhole is less than that outside. Thus, the pinholes resulted from the lack of the Al element. Because there was no Mg and F element loss, the pinholes most likely occur at the process of the substrate heating. The Al/MgF_2 pinholes resembled the craters made by exploding shells. Air may be buried by the Al films, air bubbles exploded when the substrate was heated, and some Al films were blown out. The mechanism of occurrence of the pinhole in Al/MgF_2 needs further theoretical simulation and experimental tests.

The pinholes were craters due to Al loss in the film, and they enhanced the scattering, which was the reason that they were observed [27,28]. As shown in Figs. 2(a) and 2(b), when we increased the deposition rates of the Al and substrate temperature, the pinholes slowed down the enhancement magnitude of the reflectance, and they led to the transmittance increasing for the coatings [25,26]. Thus, we made a compromise between the reflectance and the pinholes. The deposition rate of Al was chosen to be 1.0 nm/s, and the substrate temperature 200 deg. As shown in Fig. 5(a), there were no pinholes in Al/MgF_2 under this deposition condition. The measured reflectance of pinhole-free Al/MgF_2 was 63.6% at 121.6 nm [Fig. 5(b)]. In Ref. [26], the Larruquert group proposed that the increasing of the thickness of the Al films can avoid the occurrence of pinholes. We also tried their method, and we deposited the Al film with a thickness of 140 nm (Table 1, sample D5); the pinholes were still obvious [as shown in Fig. 5(c)], although the transmittance of samples we measured decreased from 10^{-5} to 10^{-7} at 700 nm (compared with Sample D1). Apparently, the increasing of the thickness of the Al film will reduce the transmittance, but this transmittance reduction does not imply that the pinholes decrease.

4. CONCLUSION

Pinholes only can be observed by dark-field microscopy and bright-field microscopy in the transmission mode; they cannot be observed by bright-field microscopy in the reflection mode. The observation by bright-field microscopy in the transmission mode requires that the substrate be double-sided polishing and transparent for visible light. Researchers seldom check the reflective mirror by this method and can be easily confused with particle contaminations. This may be the reason that the pinholes have not been visually found until now. Previous to this research, the existence of pinholes was only inferred by transmittance enhancement [26]. Since the past 80 years, this was the first time that pinholes were visually observed, and essentially, the pinhole was a pit or crater because of partial Al element loss. The existence of pinholes was dependent on the deposition rate of the Al and substrate heating temperature, and it was independent of the substrate materials. The pinholes will increase scattering, so a lower deposition rate and substrate temperatures were chosen to avoid the occurring of pinholes in Al/MgF_2. This research eliminates an otherwise easily ignored scattering source, and will contribute the most to high-precise optics, including mirrors for gyro-lasers, the detection of gravitational waves, and coronagraph detection.

Funding. Joint Fund of Astronomy (U2031122); National Natural Science Foundation of China (NSFC) (12273040).

Acknowledgment. The authors thank Professor Alexander Tikhonravov from Moscow State University for fruitful discussions of the characterization of the optical constant of MgF_2 films.

Disclosures. The authors declare no conflicts of interest.

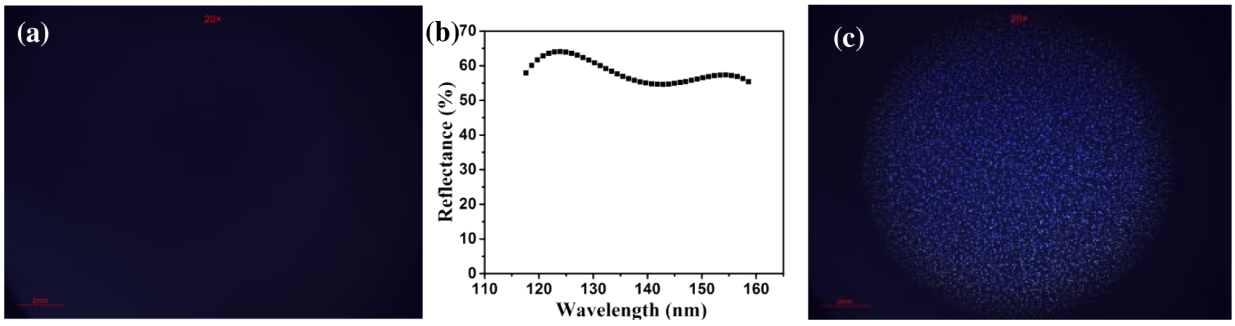

Fig. 5. (a) Surface morphology of Al/MgF_2 with a deposition rate of 1.0 nm/s and a substrate temperature of 200 deg, (b) reflectance curve of pinhole-free Al/MgF_2, and (c) pinholes in Al/MgF_2 with a thickness Al of 140 nm.

Data availability. Data underlying the results presented in this paper are not publicly available at this time but may be obtained from the authors upon reasonable request.

REFERENCES

1. Y. I. Dymshits, V. A. Korobitsyn, and A. A. Metel'nikov, "Effect of heating on the reflectivity of aluminum coatings in the vacuum ultraviolet," Sov. J. Opt. Technol. **46**, 649–651 (1979).
2. S. Wilbrandt, O. Stenzel, H. Nakamura, D. Wulff-Molder, A. Duparré, and N. Kaiser, "Protected and enhanced aluminum mirrors for the VUV," Appl. Opt. **53**, A125–A130 (2014).
3. J. I. Larruquert and R. A. M. Keski-Kuha, "Far ultraviolet optical properties of MgF_2 films deposited by ion-beamsputtering and their application as protective coatings for Al," Opt. Commun. **215**, 93–99 (2003).
4. M. Fernández-Perea, J. I. Larruquert, J. A. Aznárez, A. Pons, and J. A. Méndez, "Vacuum ultraviolet coatings of Al protected with MgF_2 prepared both by ion-beam sputtering and by evaporation," Appl. Opt. **46**, 4871–4878 (2007).
5. N. Gutiérrez-Luna, B. Perea-Abarca, L. Espinosa-Yañez, C. Honrado-Benítez, T. de Lis, L. V. Rodríguez-de Marcos, J. A. Aznarez, and J. I. Larruquert, "Temperature dependence of AlF_3 protection on far-UV Al mirrors," Coatings **9**, 428 (2019).
6. M. R. Adriaens and B. Feuerbacher, "Improved LiF and MgF_2 overcoated aluminum mirrors for vacuum ultraviolet astronomy," Appl. Opt. **10**, 958–959 (1971).
7. E. T. Hutcheson, G. Hass, and J. T. Cox, "Effect of deposition rate and substrate temperature on the vacuum ultraviolet reflectance of MgF_2- and LiF-overcoated aluminum mirrors," Appl. Opt. **11**, 2245–2248 (1972).
8. M. A. Quijada, S. Rice, and E. Mentzell, "Enhanced MgF_2 and LiF over-coated Al mirrors for FUV space astronomy," Proc. SPIE **8450**, 84502H (2012).
9. M. A. Quijada, J. del Hoyo, and S. Rice, "Enhanced far-ultraviolet reflectance of MgF_2 and LiF over-coated Al mirrors," Proc. SPIE **9144**, 91444G (2014).
10. B. Fleming, M. Quijada, J. Hennessy, A. Egan, J. del Hoyo, B. A. Hicks, J. Wiley, N. Kruczek, N. Erickson, and K. France, "Advanced environmentally resistant lithium fluoride mirror coatings for the next generation of broadband space observatories," Appl. Opt. **56**, 9941–9950 (2017).
11. L. R. Marcos, B. Fleming, J. Hennessy, D. Chafetz, J. Del Hoyo, M. Quijada, M. Bowen, D. Vorobiev, and B. Indahl, "Advanced Al/eLiF mirrors for the SPRITE CubeSat," Proc. SPIE **12188**, 1218820 (2022).
12. M. A. Quijada, L. V. Rodriguez de Marcos, J. G. Del Hoyo, E. Gray, E. J. Wollack, and A. Brown, "Advanced Al mirrors protected with LiF overcoat to realize stable mirror coatings for astronomical telescopes," Proc. SPIE **12188**, 121881V (2022).
13. H. W. Moos, S. R. McCandliss, and J. W. Kruk, "FUSE: lessons learned for future FUV missions," Proc. SPIE **5488**, 1–12 (2004).
14. J. Hennessy and S. Nikzad, "Atomic layer deposition of lithium fluoride optical coatings for the ultraviolet," Inorganics **6**, 46 (2018).
15. J. Hennessy, K. Balasubramanian, C. S. Moore, A. D. Jewell, S. Nikzad, K. France, and M. Quijada, "Performance and prospects of far ultraviolet aluminum mirrors protected by atomic layer deposition," J. Astron. Telesc. Instrum. Syst. **2**, 041206 (2016).
16. J. Hennessy, A. D. Jewell, C. S. Moore, A. G. Carver, K. Balasubramanian, K. France, and S. Nikzad, "Ultrathin protective coatings by atomic layer engineering for far ultraviolet aluminum mirrors," Proc. SPIE **10699**, 1069902 (2018).
17. S. Stempfhuber, N. Felde, S. Schwinde, M. Trost, P. Schenk, S. Schröder, and A. Tünnermann, "Influence of seed layers on optical properties of aluminum in the UV range," Opt. Express **28**, 20324–20333 (2020).
18. J. I. Larruquert, C. Honrado-Benitez, N. Gutierrez-Luna, Á. Rios-Fernandez, and P. Lopez-Reyes, "Far UV-enhanced Al mirrors with a Ti seed film," Opt. Express **29**, 7706–7712 (2021).
19. X. Zhang, B. Chen, F. He, *et al.*, "Wide-field auroral imager onboard the Fengyun satellite," Light Sci. Appl. **8**, 47 (2019).
20. M. R. Torr, D. G. Torr, M. Zukic, R. B. Johnson, J. Ajello, P. Banks, K. Clark, K. Cole, C. Keffer, G. Parks, B. Tsuratani, and J. Spann, "A far ultraviolet imager for the International Solar-Terrestrial Physics Mission," Space Sci. Rev. **71**, 329–383 (1995).
21. B. Chen, H. Li, K. Song, *et al.*, "The Lyman-alpha Solar Telescope (LST) for the ASO-S mission-II. design of LST," Res. Astron. Astrophys. **19**, 159 (2019).
22. S. N. Osterman, E. Wilkinson, J. C. Green, and K. W. Redman, "FUV grating performance for the cosmic origins spectrograph," Proc. SPIE **4013**, 360–366 (2000).
23. G. Hass and R. Tousey, "Reflecting coatings for the extreme ultraviolet," J. Opt. Soc. Am. **49**, 593–602 (1959).
24. W. R. Hunter, J. F. Osantowski, and G. Hass, "Reflectance of aluminum overcoated with MgF_2 and LiF in the wavelength region from 1600Å to 300Å at various angles of incidence," Appl. Opt. **10**, 540–544 (1971).
25. M. A. Quijada, J. G. Del Hoyo, E. Gray, J. G. Richardson, A. Howe, L. R. de Marcos, and D. A. Sheikh, "Influence of evaporation rate and chamber pressure on the FUV reflectance and physical characteristics of aluminum films," Proc. SPIE **11819**, 118190G (2021).
26. L. V. R. De Marcos, J. I. Larruquert, J. A. Méndez, N. Gutiérrez-Luna, L. Espinosa-Yáñez, C. Honrado-Benítez, J. Chavero-Royán, and B. Perea-Abarca, "Optimization of MgF_2–deposition temperatura for far UV Al mirrors," Opt. Express **26**, 9363–9372 (2018).
27. R. J. Schumacher and W. R. Hunter, "Thin aluminum filters for use on the Apollo Telescope Mount XUV spectrographs," Appl. Opt. **16**, 904–908 (1977).
28. W. R. Hunter, J. D. Purcell, and G. N. Steele, "Evaluation of pinholes in unbacked metal film filters to be used in rocket- and satellite-borne XUV spectroheliographs," Appl. Opt. **12**, 1874–1879 (1973).
29. H. Wang, X. Wang, B. Chen, Y. Wang, and S. Mao, "EUV multilayer mirrors in solar X-EUV imager," Optik **204**, 164213 (2020).